INDEX COPERNICUS INTERNATIONAL

Bio-Algorithms and Med-Systems

WWW.BAMSJOURNAL.COM ISSN: 1896-530X

ORIGINAL ARTICLE

Received: 03.12.2023
Accepted: 21.12.2023
Published: 31.12.2023

CITE THIS ARTICLE AS:
Georgadze A, Shivani, Ardebili KT, Moskal P, "Optimization of the WLS design for positron emission mammography and Total-Body J-PET systems," BAMS vol. 1, no. 1, pp. 114-123, 2023, DOI: 10.5604/01.3001.0054.1942

AUTHORS' CONTRIBUTION:
A – Study Design
B – Data Collection
C – Statistical Analysis
D – Manuscript Preparation
E – Literature Search
F – Funds Collection

CORRESPONDING AUTHOR:
Anzori Georgadze; Institute for Nuclear Research of the NAS of Ukraine, Kyiv, Ukraine; E-mail: a.sh.georgadze@gmail.com

Optimization of the WLS design for positron emission mammography and Total-Body J-PET systems

Anzori Georgadze[1,2] (ORCID: 000-0003-3512-1497), Shivani[3], Keyvan Tayefi Ardebili[4,5,6,7] (ORCID: 0000-0001-8764-1588), Paweł Moskal[3,6,7] (ORCID: 0000-0002-4229-3548)

[1]Institute for Nuclear Research of the NAS of Ukraine, Kyiv, Ukraine
[2]Institute of Physics, University of Tartu, Tartu, Estonia
[3]Faculty of Physics, Astronomy, and Applied Computer Science, Jagiellonian University, Krakow, Poland
[4]Doctoral School of Exact and Natural Science, Jagiellonian University, Krakow, Poland
[5]Faculty of Physics, Astronomy, and Applied Computer Science, Jagiellonian University, Krakow, Poland
[6]Total-Body Jagiellonian-PET Laboratory, Jagiellonian University, Krakow, Poland
[7]Center for Theranostics, Jagiellonian University, Krakow, Poland

ABSTRACT

Total-body positron emission tomography (PET) instruments are medical imaging devices that detect and visualize metabolic activity in the entire body. The PET scanner has a ring-shaped detector that surrounds the patient and detects the gamma rays emitted by the tracer as it decays. Usually these detectors are made up of scintillation crystals coupled to photodetectors that convert the light produced by the scintillation crystal into electrical signals. Jagiellonian Positron Emission Mammograph (J-PEM) is the first J-PET prototype module based on a novel idea with a plastic scintillator and wavelength shifter (WLS). At the same time, it is a prototype module for the Total-Body J-PET system. J-PEM can be an effective system for the detection and diagnosis of breast cancer in its early stage by improving sensitivity. This can be achieved using the superior timing properties of plastic scintillators combined with the WLS sheets readout. In this paper we present an application of the Geant4 program for simulating optical photon transport in the J-PEM module. We aim to study light transport within scintillator bars and WLS sheets to optimize gamma-ray hit position resolution. We simulated a pencil beam of 511 keV photons impinging the scintillator bar at different locations. For each condition we calculated the value of the pulse height centroid and the spread of the photon distribution. Some free parameters of the simulation, like reflectivity and the effective attenuation length in the sheet, were determined from a comparison to experimental data. Finally, we estimated the influence of the application of WLS layer in the Total-Body J-PET on the scatter fraction. To optimize the performance of the J-PEM module we compared geometry WLS strips 50 and 83. It was found that spatial resolution was 2.7 mm and 3.5 mm FWHM for 50 and 83 WLS strips, respectively. Despite the better granularity, the 83-strip WLS geometry

exhibited poorer resolution due to fewer photons being transmitted to the strip, resulting in large fluctuations of signal.

KEYWORDS

WLS, J-PET, total-body PET, medical imaging, J-PEM

INTRODUCTION

The technology of PET, especially total-body PET, has been under intense development in recent years, with numerous research groups committed to improving its resolution and reducing its costs [1–12]. These collective efforts aim to enhance the precision and clarity of PET imaging, contributing to its effectiveness in diagnosing and monitoring various medical conditions. The latest state-of-the-art total-body PET scanners illustrate this progress, offering cutting-edge tools for comprehensive imaging and diagnostics [3–6]. This article focuses on the PEM system [13–17], which is a PET system consisting of two modules for the detection of breast cancer. By utilizing dual modules, the PEM system offers a comprehensive and detailed examination, emphasizing its potential to significantly contribute to the early detection and precise localization of breast cancer, thereby advancing the field of breast imaging and healthcare diagnostics.

The purpose of the presented investigations is to characterize and optimize the performance of the Jagiellonian Positron Emission Mammography (J-PEM) detector, designed for the diagnosis of breast cancer. This detector incorporates a unique combination of plastic scintillator and wavelength shifter (WLS) technologies specifically engineered to enhance spatial resolution in total-body PET and J-PEM imaging systems [18–22]. One of the imaging modalities we discuss is J-PEM, designed specifically for breast cancer diagnosis. This modality employs specialized equipment featuring two parallel photon detectors arranged in a configuration similar to mammography compressors [22]. Each detector consists of two layers of plastic scintillators with wavelength shifters placed orthogonally between them. For signal detection, a SiPM (silicon photo-multiplier) is connected to both ends of each scintillator bar in the case of plastic scintillators. In the case of wavelength shifting (WLS), SiPMs are used for readout on one side, while reflective foil is employed on the other side. Our extensive studies from the J-PET experiment have provided valuable insights into the properties of plastic scintillators [18–27]. Plastic scintillators are favored for their affordability and high timing resolution (around 100 ps), with a decay time of 1.8 ns. However, their gamma quantum detection performance is notably lower than inorganic crystals. To compensate, we increased the length and thickness of the scintillator segments due to the large light attenuation lengths (typically 100–400 cm) [15].While this approach provides precise measurements of time differences at 100 ps (FWHM), it results in only moderate position resolution, approximately 7.5 mm (FWHM) [4, 16]. This estimate takes into account the slower speed of light propagation in a scintillator strip compared to a vacuum. Consequently, there also have been studies done for wavelength shifter (WLS) strips to capture scintillation light as it exits the scintillator strips, thereby improving position resolution approximately 5 mm [28, 29]. These WLS strips, made of plastic, absorb photons at higher wavelengths and reemit light isotropically at lower energies, offering useful modes for light collection. These secondary photons get trapped within the WLS strips and propagate toward the edges through total internal reflection. At the end of these strips a SiPM is placed to detect the photons. The determination of the interaction position along the *z*-axis is then estimated based on a weighted average of the *z*-coordinates of the WLS strips, where the weights correspond to the amplitudes of signals recorded in the WLS strips and are proportional to the quantities of absorbed scintillation photons. As for the position of the interaction point along the *y*-axis, it is ascertained from the number of WLS strips that capture the photons. Fig. 1. illustrates the principle of measuring the axial coordinate of the gamma quantum interaction point in a plastic scintillator bar using an array of WLS strips.

In this paper, we perform a Monte Carlo simulation using the Geant4 toolkit of light transport in the J-PEM prototype for optimization of detector geometry. We study the effect of light sharing between scintillator strips inside the module and the effect of optical surfaces selection on the accuracy of reconstruction of gamma-ray hit position. We also investigate the longitudinal response uniformity of the J-PEM block when exposed to monoenergetic 511 keV gamma rays.

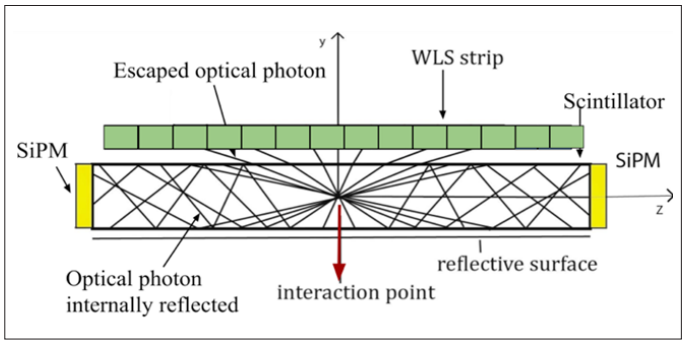

Fig. 1. A schematic view of the light inside a plastic scintillator with WLS strips. Black lines represent the light trajectories inside the plastic scintillator [28].

MATERIAL AND METHODS

Geometry of J-PEM

Design of the J-PEM system consists of two modules of plastic scintillators described in [22, 25]. Each module is built from two layers of plastic scintillator with the wavelength shifters placed orthogonally between them, as shown in Fig. 2. Each scintillator bar is attached at both ends to silicon photomultipliers for the signal readout.

The combined use of plastic scintillators, which have superior timing properties, with the WLS strips can provide an affordable and precise scanner with significant improvement in spatial resolution and efficiency for the detection of breast cancer.

For optimizing the J-PEM detector we simulated geometry consisting of 32 plastic scintillator strips BC-404 measuring 500 × 24 × 6 mm³ arranged in two rows with 16 scintillator strips in each (see Fig. 2.). Between the scintillators were placed WLS strips, which absorbed the light from scintillators. The light yield of this plastic scintillator was 10,400 photons per MeV of deposited energy, density was 1.032 g/cm^3, absorption length 140 cm, refractive index 1.58 and Birk's constant 0.126 mm/MeV [30]. To prevent light leakage the scintillator was wrapped in two different types of foils. The first layer utilized Vikuiti 3M, an enhanced secular reflector (ESR) known for its ultrahigh reflectivity and mirrorlike optical polymer film. The second layer was done using Kapton 100B DuPont to make the setup light-tight. In our detector we employed BC-482A as the wavelength shifter, which was a green-emitting WLS plastic specifically designed for shifting the emission spectra of common blue scintillators (BC-404). WLS strips in the J-PEM had reflecting Vikuiti foils on two sides measuring 100 mm × 3 mm (covering the side surfaces between the WLS), and on one side there were foils measuring 3 mm ×10 mm, opposite the SiPM.

To assess the impact of the WLS strips geometry of position resolution of the J-PEM module we performed a simulation of two geometries. One module geometry consisted of 50 WLS strips (100 × 3 × 9.9) mm^3 and readout on one side by one or two 3 × 3 mm^2 SiPMs. The other geometry consisted of 83 WLS strips (100 × 3 × 5.9) mm^3. By arranging a large number of WLS strips we expected to obtain better spatial resolution along the z-axis, which is parallel to the scintillator strip.

Geant4 simulation of light transport from scintillator to wavelength shifting sheets

We performed a full Monte Carlo simulation of the response of a J-PEM module composed of scintillator bars with a WLS sheet light readout, and the number of WLS strips was 50 and 83. A complete Monte Carlo model of a scintillator included a coupled ionizing particle and optical photon transport, which could be simulated with the GEANT4 and GATE v6.2 packages [31–33].

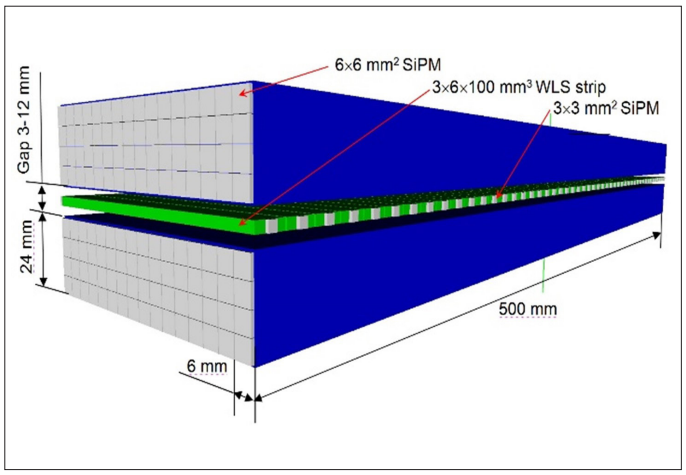

Fig. 2. Perspective projection of the J-PEM module. Blue indicates plastic scintillators, green indicates wavelength shifters, and gray indicates SiPMs.

For optical photon transport, GEANT4 uses the concept of optical surfaces to describe light reflection and transmission at the boundary between two media. The developed simulation model was tested against laboratory data [29] obtained for the light response of both the scintillator and the WLS sheet.

All relevant physical processes were considered in the physics list of Geant4 simulation. Standard electromagnetic processes, e.g. ionization, bremsstrahlung, multiple scattering, pair production, Compton scattering and photoelectric effect were considered. Optical processes included scintillation, Cherenkov radiation, volume absorption, Rayleigh scattering and boundary processes (reflection, refraction, absorption). The dominant photon generation process was scintillation, in which it was important to activate Birk's effect. The interface was modeled as polished, and the boundary processes followed the rules of the GLISUR model. In this model the user could select the smoothness or roughness of each surface surrounding the scintillator using a parameter named polish. If polish equaled zero this case corresponded to the maximum roughness (photons were reflected according to a Lambertian distribution), whereas for polish equal to one Snell's Law was applied. For each surface appropriate optical boundary processes were specified and reflectivity was defined. Necessary optical input parameters were adopted as follows. The surface type was dielectric_dielectric for scintillator and WLS strips, photodiodes and the ESR reflector. For all grease-coupled surfaces, dielectric_dielectric was set as a surface type with the glisur model so as to use the Fresnel formulas for optics calculation. The surface finish was set to polish for the glisur model. According to [34], the reflectance of ESR film was set to 98% across the whole wavelength range of interest. To keep the scintillator strips and the WLS sheets in light-tight housing, the dielectric_metal with the glisur model (reflectivity: 0; quantum efficiency: 100%) was defined as a photon absorber attached to the outermost layer.

In order to count the photoelectrons in the scope of this work, Hamamatsu S13360 type SiPM was used as a benchmark unit [35].

The detection efficiency of the SiPM was determined by weighting the SiPM PDE with the BC-404 emission spectra, which gave a value of ~40%.

RESULTS AND DISCUSSION

Impact of WLS layer geometry on the position resolution of the Total-Body J-PET scanner

The detailed simulations of the J-PEM module were performed in [22, 34]. In this research, we focused on optimization detector geometry to obtain best performance. In the proposed geometry the scintillator was wrapped only from three sides. One side of the WLS strip, facing the WLS strip, was not covered, allowing optical photons to travel toward the WLS strip medium. Efficient light transport from the scintillator to the WLS sheet depended on factors such as the refractive index of the scintillator and the WLS sheet and the distance between them. Light first escaping the scintillator entered air media with a refraction index equal to 1, and then entered WLS media with a higher refractive index. As a result, some optical photons were reflected back to the scintillator but some started propagation in an air gap between the scintillator and the WLS strips, thus penetrating other neighboring strips. Detection of these would result in gamma-ray hit detection failures and image deterioration.

This effect is explained in Fig. 3. In Fig. 3. (left), a gamma-ray with energy 511 keV hits the scintillator strip with the number 9, counting from the left. In Fig. 3. (right), gamma-ray 511 keV interacted with scintillator strips of the J-PET module twice, which made malefaction in gamma-ray direction determination. The effect of light sharing in the scintillator-WLS structure of the J-PET module can also lead to the simultaneous detection of signals in two strips. Therefore, we studied this effect by simulating with Geant4 10 million of the 400 keV electrons generated inside the scintillator strip. We did not simulate 511 keV photons in this case because they produce a double scatter event on the module, thus mimicking the effect of the double hits produced by the effect of light sharing. In the modeling procedure a threshold of 10 photoelectrons was set, simulating the threshold of electronic hardware, and the coincidence of photodetectors at both ends of the scintillation tape was considered. As a result of the simulation no hits were found in other scintillation strips except for the one with the electron source. We also simulated a pencil beam of a 10-million 511 keV photons incident on the J-PEM module to study the effect of double Compton scattering within the J-PEM module, which can lead to image degradation because, in this case, it was impossible to determine with which strip the primary photon with an energy of 511 keV interacted.

The double Compton scattering effect in the J-PEM module results in higher detection efficiency of the scintillation array, which is closer to the 511 keV gamma-ray source (Fig. 4.). Lower detection

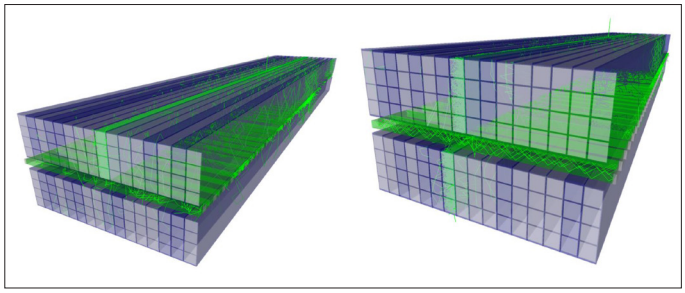

Fig. 3. (Colour online) Left: visualization of optical-photon-sharing between scintillator strips for the case of a one-gamma-ray scatter event. Right: visualization of optical-photon-sharing between scintillator strips for the case of a double-gamma-ray scattering event.

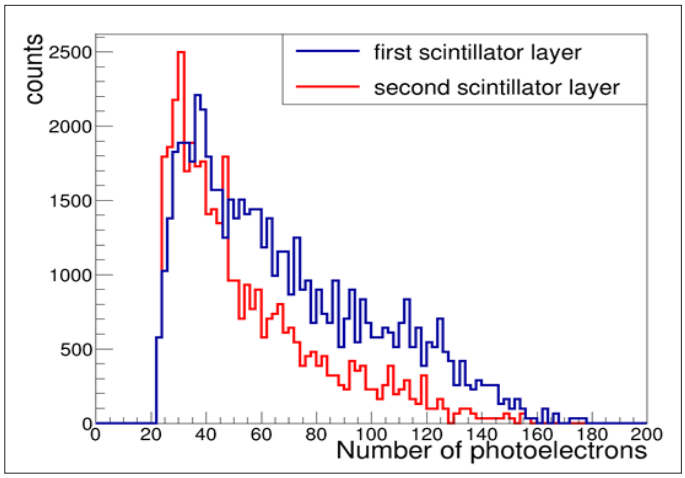

Fig. 4. Comparison of distribution of photons detected in the first scintillator array closer to the gamma-ray source and the second scintillator array, which was farther away from the source.

efficiency of the second scintillation array, which is behind the first, is a result of the effect of hardware threshold, which eliminates scatter events with energy less than threshold value, thus leaving them undetected in the second array. For each registered event the distribution of amplitudes of WLS pulses presented as a function of the WLS coordinates was analyzed using a high-resolution peak search function from the ROOT data analysis package [35] and then fitted with a Gaussian function.

The center of the function was taken as the reconstructed position of the gamma quantum interaction point. To assess the impact of the number of WLS strips on the position resolution we simulated the geometry with 50 WLS strips and 83 WLS strips between scintillator strips. The modeling results for the first point of view were unexpected. It was found that better granularity with 83 WLS strips did not result in better position resolution. Fig. 5. presents the distributions of reconstructed z–coordinates of the gamma-quantum interaction for two different positions of the ^{22}Na source differing by Δz = 5 mm for cases of 50 and 83 WLS strips. One can see that position resolution is of the same order, about 3-mm FWHM for both geometries. We explain this effect as the result of a smaller cross section of WLS strips for geometry

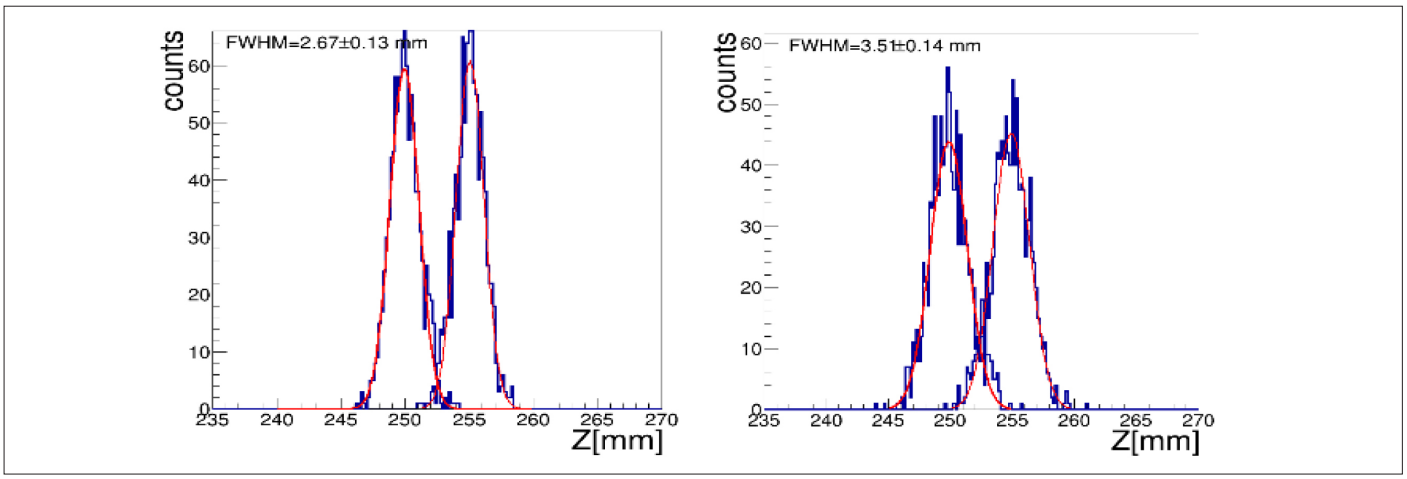

Fig. 5. Left: distributions of reconstructed z–z-coordinates of the gamma quantum interaction for two different irradiation positions differing by Δz = 5 mm for the case of 50 WLS strips used with dimensions 100 × 3 × 9.9 mm^3 readout, with SiPM 3 × 3 mm^2. Right: distributions of reconstructed z–z-coordinates of the gamma quantum interaction for two different irradiation positions differing by Δz = 5 mm with 83 WLS strips used with dimensions 100 × 3 × 5.9 mm^3 readout with SiPM 3 × 3 mm^2. The blue curve is simulated results and the red curve is Gaussian fitting.

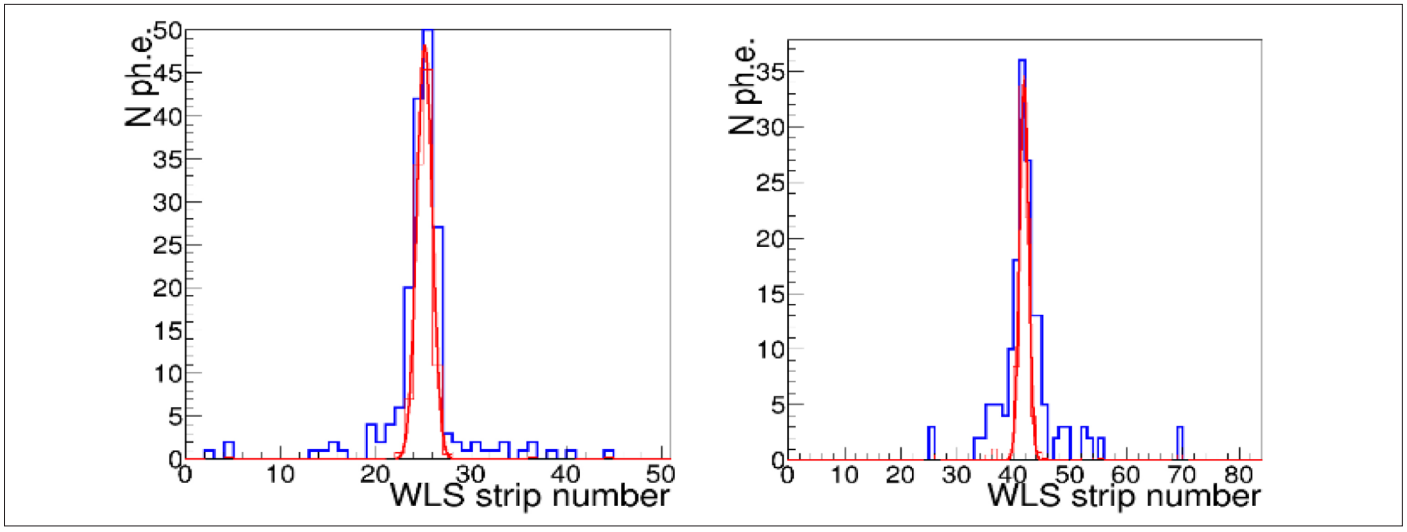

Fig. 6. Left: detected photoelectrons in 50 WLS strips geometry for a typical event. Gaussian fits to the data lead to determining the coordinate of the gamma-quantum interaction point. Right: amplitudes measured in individual 83 WLS strips. The blue curve is simulated results and the red curve is Gaussian fitting.

with 83 strips. As a result, a smaller number of scintillation photons were absorbed in the WLS strip. Besides, reemitted green photons underwent more scatterings in a smaller-width ~ 6 mm WLS strip then in 10 mm strip. The surface roughness of the strip causes the Lambertian scattering of photons, disrupting the phenomenon of total internal reflection. As a consequence, photons are subsequently absorbed. Therefore, for 6-mm cross-section WLS strips statistical fluctuations in the number of detected photons in strips are larger than for 10-mm-wide strips (see Fig. 6.). This causes degradation of accuracy of hit-position reconstruction for 83-WLS-strip geometry. To mitigate the effect of cross section on photon propagation we considered the geometry of a WLS strip with cross dimensions of 6 × 6 × 100 mm^3.

Also, the size of SiPMs affects position resolution; therefore, we simulated the readout of WLS strips with one 3 × 3 mm^2 or two 3 × 3 mm^2 parallel to a SiPMs channel. A WLS strip with a 6 × 6 mm cross section can be a readout with a 6 × 6 mm^2 SiPM. Fig. 7. shows that using two SiPMs with a total detection area of 3 × 6 mm^2 improved light collection, which resulted in better position resolution for both 50 and 83 WLS strip geometries. The distance between the scintillator and the WLS sheet can also play a role in light-transport efficiency. If the separation is too large some of the light may not be fully absorbed and reemitted by the WLS sheet, leading to reduced detection efficiency. Conversely, if the separation is too small some of the WLS sheet fluorescence may be reabsorbed by the scintillator, leading to reduced efficiency. Fig. 8. presents results of the simulation for WLS strip geometry, 6 × 6 × 100 mm^3.

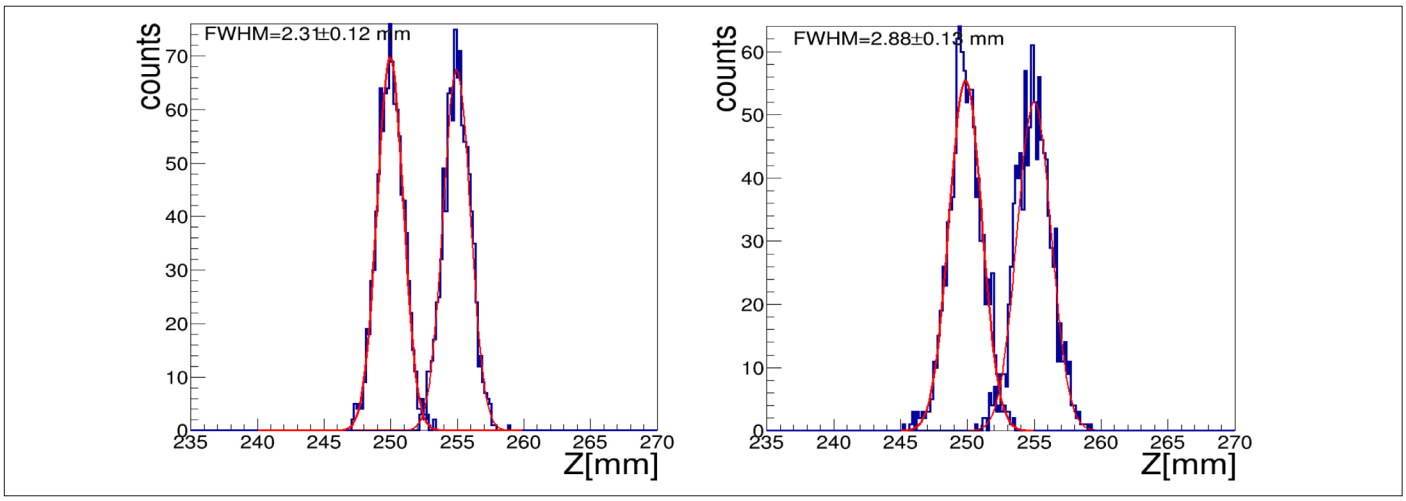

Fig. 7. Left: distributions of reconstructed z–z-coordinates of the gamma quantum interaction for two different interaction positions differing by Δz = 5 mm for the case of 50 WLS strips with dimensions 100 × 3 × 9.9 mm^3 readout with 2 SiPMs 3 × 3 mm^2. Right: distributions of reconstructed z–z-coordinates of the gamma quantum interaction for two different positions with 83 WLS strips with dimensions 100 × 3 × 5.9 mm^3 readout with 2 SiPMs 3 × 3 mm^2. The blue curve is the simulated results and the red curve is Gaussian fitting.

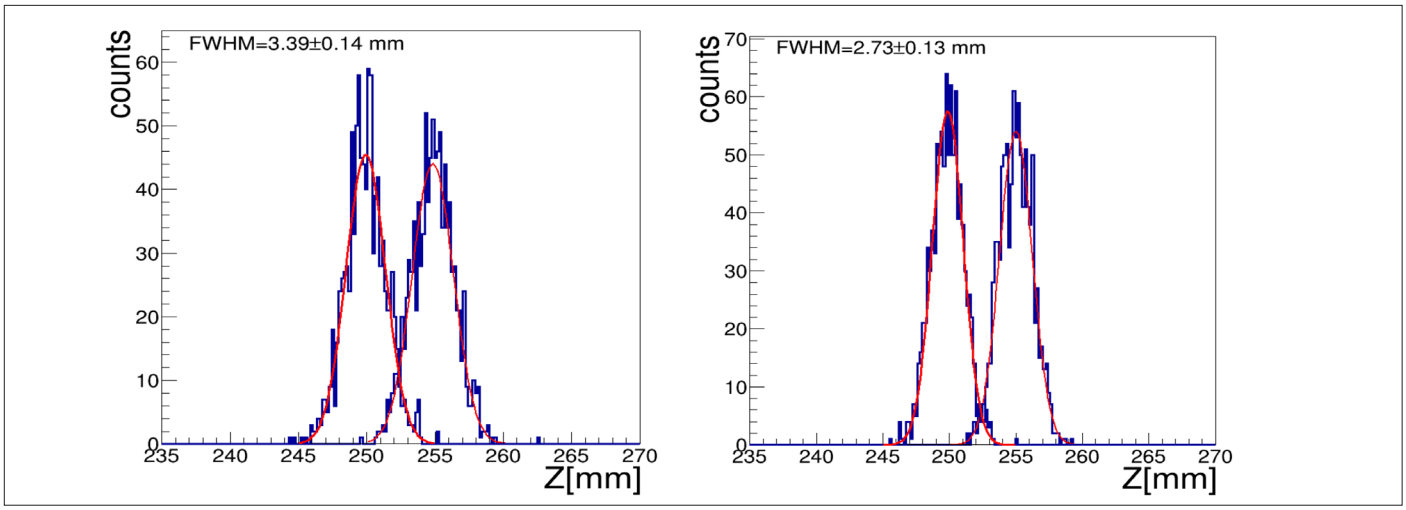

Fig. 8. Left: distributions of reconstructed z–z-coordinates of the gamma quantum interaction for two different irradiation positions differing by Δz = 5 mm for the case of 83 WLS strips with cross sections 6 × 6 mm^2 readout with 3 × 3 mm^2 SiPM. Right: distributions of reconstructed z–coordinates of the gamma quantum interaction for two different positions, with a 83 WLS strips readout with 6 × 6 mm^2 SiPM. The blue curve is the simulated results and the red curve is Gaussian fitting.

Another aspect of this research was a study of the effect of wrapping the WLS strips with reflective material. We simulated a pencil beam of 1 million 511 keV photons incident on the central scintillator strip at 250 mm and 255 mm and compared the position resolution of the J-PEM module for the two cases when no reflective material was inserted inside the air gap between the WLS strips and when ESR reflective material was inserted between them (Fig. 8.). Therefore, we also investigated the effect of the distance between the scintillation strip arrays between which the WLS strips were installed. This was necessary to refine the module geometry, comparing the geometry with the best physical parameters with the geometry based on mechanical requirements, taking into account the parameters of the supporting structure.

We simulated a pencil beam of 1 million 511 keV photons incident on the central scintillator strip at the positions 250 mm and 255 mm and compared the position resolution of the J-PEM module for the two cases when the distance between the scintillator strip arrays was 3.2 mm, which was an air gap between the WLS strips and the arrays of 0.1 mm. In the second configuration the distance between the scintillator strip arrays was 12 mm.

In Fig. 9. the distributions of reconstructed z–coordinates of the gamma quantum interaction for two different positions of the 511 keV photons differing by Δ z = 5 mm with 3.2- and 12-mm distance (indicated as a parameter gap in Fig. 2.) between scintillator arrays are shown. It can be seen that position resolution, as expected, was better for smaller distances between scintillator strip arrays.

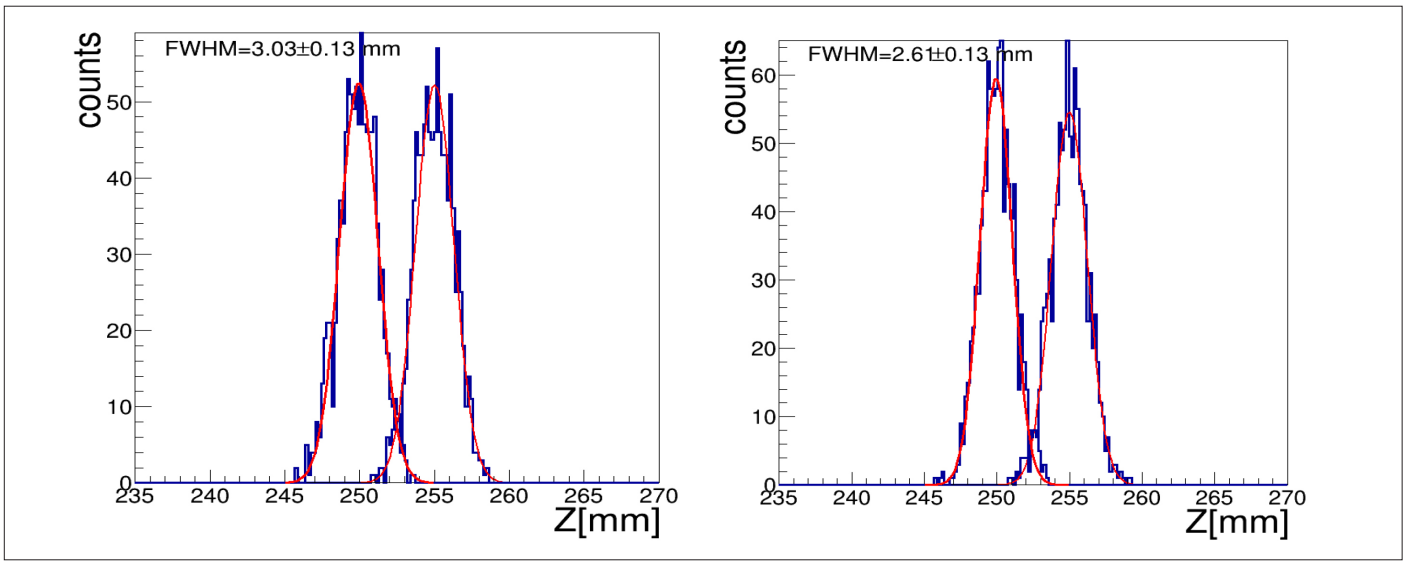

Fig. 9. Left: distributions of reconstructed z–coordinates of the gamma quantum interaction for two different interaction positions differing by Δz = 5 mm without reflective material between the WLS strips. Right: distributions of reconstructed z–coordinates of the gamma quantum interaction for two different interaction positions differing by Δz = 5 mm with ESR reflective material inserted between the WLS strips. The blue curve is the simulated results and the red curve is Gaussian fitting.

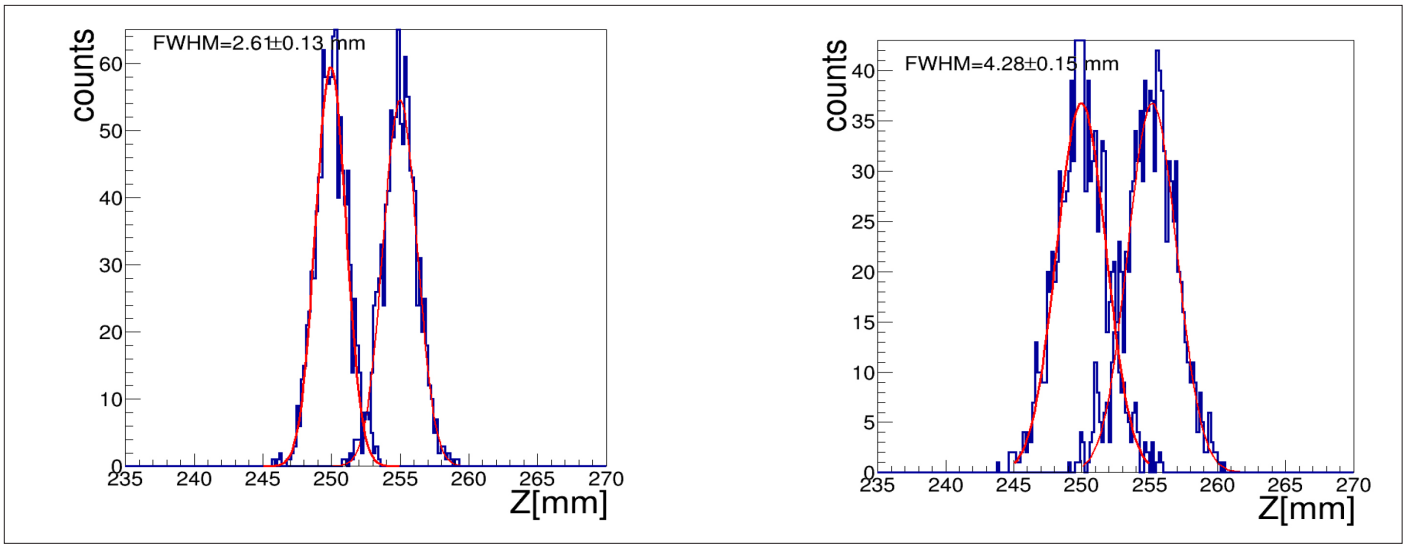

Fig. 10. Left: distributions of reconstructed z–coordinates of the gamma quantum interaction for two different interaction positions differing by Δz = 5 mm with a 3.2-mm distance between the scintillator arrays. Right: distributions of reconstructed z–coordinates of the gamma quantum interaction for two different interaction positions differing by Δz = 5 mm with a 12 mm-distance between the scintillator arrays

We have studied the uniformity of the response of the J-PEM module to different longitudinal gamma-ray exposure locations, and this study reveals the effect by the simulation of optical photon propagation in a hole J-PEM module. To test the response uniformity of the J-PEM module we simulated a pencil beam of 1 million 511 keV photons incident strip at 250 mm and 255 mm on the first scintillator strip, and on the ninth strip in the array. We also repeated these simulations for a pencil beam incident at the positions 450 mm and 455 mm of these strips.

The resulting distributions of reconstructed z–coordinates for these gamma ray beams are shown in Fig. 11.

Impact of WLS layer thickness on scatter fraction in the Total-Body J-PET scanner

The Total-Body J-PET scanner comprises seven rings, each consisting of 24 modules (see Fig. 12.). A single module consists of three layers. The first and third layers include 16 plastic scintillator strips, each with a length of 33 cm, positioned adjacent to each other. The second layer incorporates 50 WLS bars, placed between the two plastic layers and perpendicular to them [37].

The scatter fraction assesses the detector's sensitivity to scattered radiation [2, 4, 6, 37]. In this study simulations were conducted

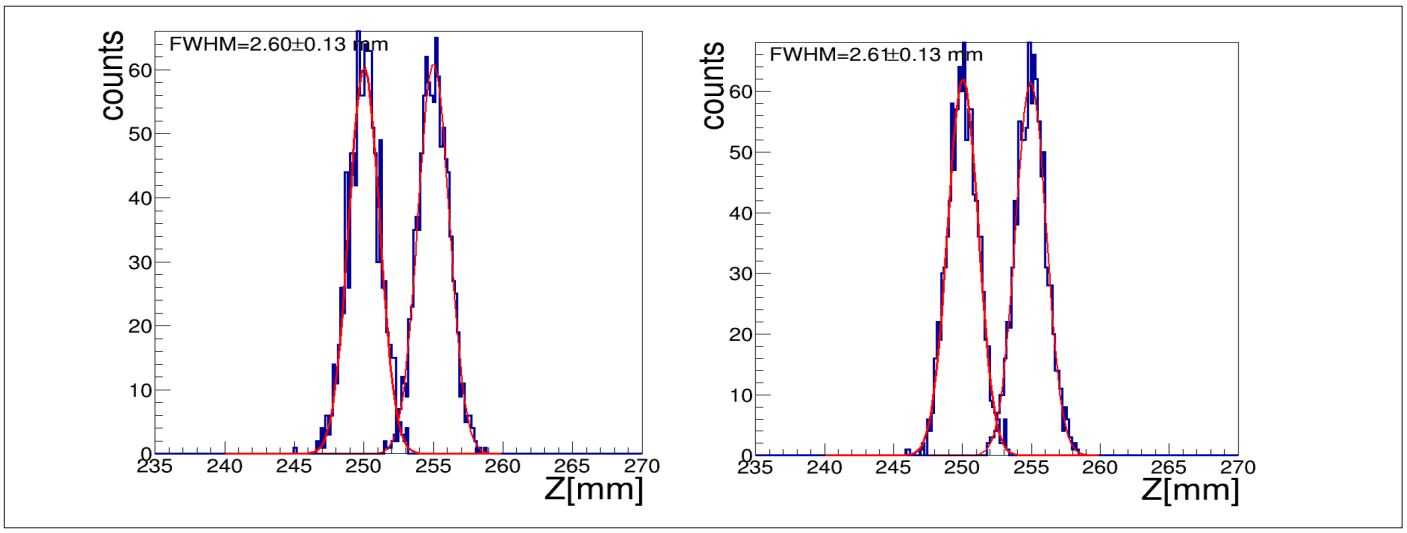

Fig. 11. Top left: distributions of reconstructed z–z-coordinates of the gamma quantum interaction in the first scintillator strip in an array for two positions at 250 mm and 255 mm. Top right: the same distributions for the ninth scintillator strip for two positions at 250 mm and 255 mm. Bottom left: distributions of reconstructed z– z-coordinates of the gamma quantum interaction in the first scintillator strip in an array for two positions at 450 mm nd 455 mm. Bottom left: distributions of reconstructed z– z-coordinates in the ninth scintillator strip for two positions at 450 mm and 455 mm.

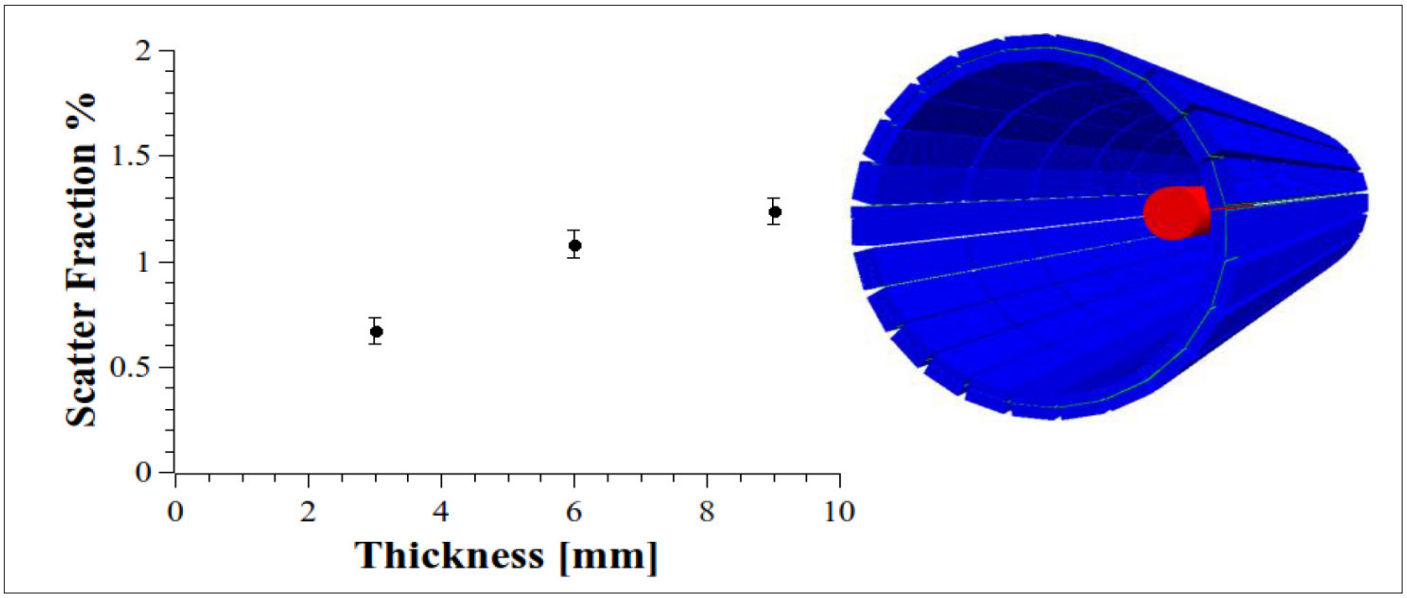

Fig. 12. Left: scatter fraction ratio in various thicknesses of a WLS layer. Right: schematic view of the simulated Total-Body J-PET and scatter fraction phantom in the center of the scanner.

using GATE [38, 39] version 9 to evaluate the impact of the WLS layer with thicknesses of 3 mm, 6 mm, and 9 mm on the scatter fraction of the Total-Body J-PET. The simulations focused on Total-Body J-PET with the presence of a WLS layer at various thicknesses and without a WLS layer. The scatter phantom was employed with a back-to-back annihilation photon source with an activity of 1 MBq. The analysis followed the methodology outlined in the reference [37]. Fig. 12. (left) illustrates the results, showing the scatter fraction for different thicknesses of the WLS layer in comparison with the absence of the WLS layer. The results of the simulations are summarized in Tab. I.

CONCLUSIONS

The efficient light transport from the scintillator to the WLS sheet is a critical aspect of the design and performance of scintillation detectors. In this Monte Carlo simulation study many factors affecting the performance of the light collection efficiency of the J-PEM detector module have been studied. Firstly, some free parameters of the simulation, like the reflectivity and the effective attenuation length in the sheet, were determined from a comparison to experimental data. We simulated a J-PEM module with 50 WLS strips and 83 WLS strips and found that position

Tab. I. Technical specifications of D-D neutron generator.

SIMULATED CONDITIONS	FWHM (MM)
50 WLS strips with 3 × 3 mm² SiPM	**2.67 ±0.13**
83 WLS strips with 3 × 3 mm² SiPM	3.51 ±0.14
50 WLS strips with 3 × 6 mm² SiPM	2.31 ±0.12
83 WLS strips with 3 × 6 mm² SiPM	2.88 ±0.12
83 WLS strips with cross-section 6 × 6 mm² readout with 3 × 3 mm² SiPM	3.39 ±0.14
83 WLS strips with cross-section 6 × 6 mm² readout with 6 × 6 mm² SiPM	2.73 ±0.13
ESR reflector between WLS strips	2.61 ±0.13
no ESR reflector between WLS strips	3.03 ±0.14
distance between scintillator arrays 3.1 mm	2.61 ±0.13
distance between scintillator arrays 12 mm	4.28 ±0.15
Gamma ray interaction position – center of the 1st scintillator strip	2.60 ±0.13

resolution is almost the same. We also assessed the impact of increasing the SiPM number which readout WLS strips on position resolution. It was found that position resolution is improved for both geometries with 50 WLS strips and 83 WLS strips. Then the impact of inserting reflective material between the WLS strips was investigated. It was found that the insertion of highly reflective ESR sheets does not drastically improve the position resolution of the detector module. For most scintillators the correct selection and implication of reflective coating are an issue to increase light collection. Our simulation shows that the effect of the insertion of wrapping material between WLS strips is moderate, and accurate position reconstruction is possible with an air gap between WLS strips. Also, the distance between scintillator arrays is not so crucial for the position resolution of the detector module. A common problem associated with long scintillators is that their responses are highly dependent on the gamma-ray irradiation location due to large light losses. The investigation of the longitudinal position resolution of the J-PEM module shows the uniform response to incident gamma rays at different locations on the detector module surface. Results from the simulations show the feasibility of the developed concept of a J-PEM detection module for breast cancer, thus making J-PEM a viable tool in the early detection of cancer.

REFERENCES

1. Moskal P, Stępień E. Prospects and clinical perspectives of totalbody PET imaging using plastic scintillators. PET clinics. 2020:15:439-52.
2. Moskal P, Kowalski P, Shopa RY, Raczyński L, Baran J, Chug N, et al. Simulating NEMA characteristics of the modular totalbody J-PET scanner—an economic total-body PET from plastic scintillators. Physics in Medicine & Biology. 2021;66:175015.
3. Badawi RD, Shi H, Hu P, Chen S, Xu T, Price PM, et al. First human imaging studies with the explorer total-body pet scanner. J Nucl Med. 2019;60:299.
4. Spencer BA, Berg E., Schmall JP., Omidvari N, Leung EK, Abdelhafez YG, et al. Performance evaluation of the uExplorer total-body pet/ct scanner based on NEMA-nu 2-2018 with additional tests to characterize pet scanners with a long axial field of view. J Nucl Med. 2021;61:861.
5. Dai B, Daube-Witherspoon ME, McDonald S, Werner ME, Parma MJ, Geagan MJ, et al. Performance evaluation of the PennPET explorer with expanded axial coverage. Phys Med Biol. 2023;68:095007.
6. Prenosil GA, Sari H, Fürstner M, Afshar-Oromieh A, Shi K, Rominger A, et al. Performance characteristics of the biograph vision quadra pet/ct system with a long axial field of view using the NEMA NU 2-2018 standard. J Nucl Med. 2022;63:476.
7. Alavi A, Werner TJ, Stępień EŁ, Moskal P. Unparalleled and revolutionary impact of PET imaging on research and day to day practice of medicine. Bio-Algorithms and Med-Systems. 2021;17:203-20.
8. Vandenberghe S, Moskal P, Karp JS. State of the art in total body PET. EJNMMI Phys. 2020;7:35.
9. Zein SA, Karakatsanis NA, Issa M, Haj-Ali AA, Nehmeh SA. Physical performance of a long axial field-of-view PET scanner prototype with sparse rings configuration: a Monte Carlo simulation study. Med Phys. 2020;47:1949-57.
10. Karakatsanis NA, Nehmeh MH, Conti M, Bal G, González AJ, Nehmeh SA. Physical performance of adaptive axial FOV PET scanners with a sparse detector block rings or a checkerboard configuration. Phys Med Biol. 2022;67:105010.
11. Dadgar M, Parzych S, Baran J, Chug N, Curceanu C, Czerwiński E, et al. Comparative studies of the sensitivities of sparse and full geometries of Total-Body PET scanners built from crystals and plastic scintillators. EJNMMI Physics. 2023;62:10.
12. Efthimiou N. New Challenges for PET Image Reconstruction for Total--Body Imaging. PET Clin. 2020;15:453-61.
13. Collarino A, Fuoco V, Arias-Bouda LMP, Sánchez AM, de Geus-Oei LF, Masettiet R, et al. Novel frontiers of dedicated molecular imaging in breast cancer diagnosis. Translational cancer research. 2018;7:S295-S306.
14. Soriano A, Sánchez F, Carrilero V, Pardo A, Vidal San Sebastian LF, Vazquez C, et al. Performance evaluation of the dual ring MAMMI breast PET. IEEE Nuclear Science Symposium and Medical Imaging Conference. IEEE. 2013:1-4.
15. Almeida P, Auffray E, Barbosa J, Bastos AL, Bexiga V, Bugalho R, et al. An overview of the Clear-PEM breast imaging scanner. IEEE Nuclear Science Symposium Conference Record. 2008:5616-8.
16. MacDonald L, Edwards J, Lewellen T, Haseley D, Rogers J, Kinahan P, et al. Clinical imaging characteristics of the positron emission mammography camera: PEM Flex Solo II. J Nucl Med. 2009;50:1666-75.
17. Murthy K, Aznar M, Thompson CJ, Loutfi A , Lisbona R, Gagnon JH. Results of preliminary clinical trials of the positron emission mammography system PEM-I: a dedicated breast imaging system producing glucose metabolic images using FDG. J Nucl Med. 2000;41: 1851-8.
18. Moskal P, Salabura P, Silarski M, Smyrski J, Zdebik J, Zieliński M. Novel detector systems for the Positron Emission Tomography. Bio-Algorithms and Med-Systems. 2011;7:73-8.
19. Moskal P, Rundel O, Alfs D, Bednarski T, Białas P, Czerwiński E, et al. Time resolution of the plastic scintillator strips with matrix photomultiplier readout for J-PET tomograph. Physics in Medicine & Biology. 2016;61:2025.
20. Niedwiecki S. Studies of detection of radiation with use of organic scintillator detectors in view of positron emission tomography. master thesis, Jagiellonian University, Cracow, 2011.

21. Pawlik-Niedźwiecka M. Studies of changes of signals shapes in plastic scintillator strips. PhD thesis. master thesis, Jagiellonian University, Cracow, 2014.
22. Shivani. Evaluation of Positron Emission Mammography using plastic scintillator and wavelength shifters. PhD thesis, Jagiellonian University, Cracow, 2023.
23. Niedwiecki S. Double-strip prototype of polymer time-of-flight positron emission tomograph based on multi-level analog electronics. PhD thesis, Jagiellonian University, Cracow, 2019.
24. Kaplon L. Synthesis and Characterization of Polystyrene Scintillators and Their Application in Positron Emission Tomography. PhD thesis. Jagiellonian University, Cracow, 2017.
25. Kapłon Ł. Technical attenuation length measurement of plastic scintillator strips for the total-body J-PET scanner. IEEE Transactions on Nuclear Science. 2020;67:2286-9.
26. Baran J, Chug N, Coussat A, Curceanu C, Czerwiński E, Dadgar M, et al. Comparative studies of plastic scintillator strips with high technical attenuation length for the total-body J-PET scanner. Nuclear Instruments and Methods in Physics Research Section A: Accelerators, Spectrometers. Detectors and Associated Equipment. 2023;1051:168186.
27. Moskal P, Niedźwiecki S, Bednarski T, Czerwiński E, Kapłon Ł, Kubicz E, et al. Test of a single module of the J-PET scanner based on plastic scintillators. Nucl Instrum Methods Phys Res A: Accel Spectrom Detect Assoc Equip. 2014;764:317-21.
28. Smyrski J, Moskal P, Bednarski T, Białas P, Czerwiński E, Kapłon Ł, et al. Application of WLS strips for position determination in strip PET tomograph based on plastic scintillators. Bio-Algorithms and Med-Systems. 2014;10:59-63.
29. Smyrski J, Alfs D, Bednarski T, Białas P, Czerwiński E, Dulskiet K, et al. Measurement of gamma quantum interaction point in plastic scintillator with WLS strips. Nucl Instrum Methods Phys Res A: Accel Spectrom Detect Assoc Equip. 2017;851:39-42.
30. Saint-Gobain [Internet]. Organic scintillation materials [cited 2023 Dec 03]. Available from: http://www.crystals.saint- gobain.com/uploadedFiles/SG- Crystals/Documents/SGC%20Organics%20Brochure.pdf., https://www.luxiumsolutions.com/radiation-detection-scintillators/plastic-scintillators/bc400-bc404-bc408-bc412-bc416.
31. Agostinelli S, Allison J, Amako KA, Apostolakis J, Araujo H, Arce P, et al. Geant4—a simulation toolkit. Nucl Instrum Methods Phys Res A: Accel Spectrom Detect Assoc Equip. 2003;506:250-303.
32. Geant4 Collaboration [Internet]. Geant4 User's Guide for Application Developers [cited 2023 Dec 03]. Available from: http://geant4.web.cern.ch/geant4/support/index.shtml.
33. Brun R, Rademakers F. ROOT - An Object Oriented Data Analysis Framework. Nucl Instrum Methods Phys Res A: Accel Spectrom Detect Assoc Equip. 1997;389:81-6.
34. 3M™ [Internet]. Enhanced Specular Reflector (ESR) [cited 2023 Dec 03]. Available from: https://multimedia.3m.com/mws/media/1389248O/application-guide-for-esr.pdf.
35. Hamamatsu [cited 2023 Dec 03]. Available from: https://www.hamamatsu.com/content/dam/hamamatsu-photonics/sites/documents/99_SALES_LIBRARY/ssd/s13360_series_kapd1052e.pdf.
36. Shivani S. Development of J-PEM for Breast Cancer Detection, Proc. of the 15th Int. Workshop on Slow Positron Beam Techniques and Applications, Prague, September 2–6, 2019, ACTA PHYSICA POLONICA A 2020;137:140-144.
37. Tayefi Ardebili K, Niedźwiecki S, Moskal P. Estimation of 511 keV Gamma Scatter Fraction in WLS Layer in Total-Body J-PET; A Simulation Study. Acta Phys Pol B. 2022;15:4-A7.
38. Sarrut D, Bała M, Bardiès M, Bert J, Chauvin M, Chatzipapas K. et al. Advanced Monte Carlo simulations of emission tomography imaging systems with GATE. Phys Med Biol. 2021;66:10TR03.
39. Sarrut D, Baudier T, Borys D, Etxebeste A, Fuchs H, Gajewski J, et al. The OpenGATE ecosystem for Monte Carlo simulation in medical physics. Phys Med Biol. 2022;67:184001.